ELSEVIER

S0032-3861(96)00613-1

Polymer Vol. 38 No. 5, pp. 1047–1055, 1997

0032-3861/97/$17.00 + 0.00

Micromechanical and microdielectric transitions in P(S-*g*-EO) modified PPO/PMMA blends

H. Eklind and F. H. J. Maurer*
Department of Polymer Technology, Chalmers University of Technology, S-41296 Göteborg, Sweden

and P. A. M. Steeman
DSM Research BV, PO Box 18, NL-6160 MD Geleen, The Netherlands
(Received 19 January 1996; revised 27 May 1996)

The effect of two poly(styrene-*graft*-ethylene oxide)s with different graft lengths and graft densities on the interphase properties of poly(2,6-dimethyl-1,4-phenylene oxide)/poly(methyl methacrylate) (PPO/PMMA) blends was studied by different techniques. The miscibility between the copolymers and the homopolymers, as well as the phase reduction in the ternary blends, was favoured by longer and more separated grafts. Transmission electron microscopy shows that the addition of any of the copolymers leads to the formation of an interphase between the heterogeneous PPO and PMMA phases. The ternary blends present micromechanical and microdielectric transitions at temperatures in the range 60–100°C, where the transition temperatures decrease with increasing copolymer contents. The micromechanical and microdielectric transitions originate from the change in the relative moduli values and the dielectric losses of the matrix, interphase and particle phase of the ternary blends.

(Keywords: interphase; micromechanical transition; microdielectric transition)

INTRODUCTION

The properties of polymer blends are strongly influenced by the existence and properties of the interphase. As most polymer pairs are immiscible and form heterogeneous systems with narrow interphases, the stress transfer across the phase boundaries is limited, which results in weak mechanical properties of the blend material. The addition of a small amount of compatibilizer to an immiscible polymer blend is often a powerful means for increasing the interaction between the phases, and thus the mechanical properties, by the formation of a strong interphase. Several studies[1–4] have shown that an efficient compatibilizer should be located mainly at the interphase between the immiscible polymers and increase the interaction and enlarge the interphase volume between the phases. Another effect of the compatibilizer is a reduced interfacial energy between the phases, which permits a more stable and finer dispersion[5–7], giving a morphology that is less sensitive to processing conditions.

Different techniques have been used previously[8–11] to study the influence of a graft copolymer [P(S-*g*-EO)], with polystyrene (PS) backbones and poly(ethylene oxide) (PEO) side chains, on the properties of poly(2,6-dimethyl-1,4-phenylene oxide)/poly(methyl methacrylate) (PPO/PMMA) blends. Scanning electron microscopy (SEM) shows that the dispersed (PPO) phase size in a PPO/PMMA 30/70 blend decreases when the copolymer is added, and the reduction is larger when more copolymer is added. The experiments thus indicate that P(S-*g*-EO) has a high interfacial activity in the PPO/PMMA system, which can be explained by favourable interactions between PS/PPO and PEO/PMMA, respectively. Dynamic mechanical measurements show an, at first, unexpected behaviour: a small addition (1–10 volume parts) of P(S-*g*-EO) to a PPO/PMMA 30/70 blend results in a new transition at 60–100°C, with a position depending on the amount of P(S-*g*-EO) added. This additional transition cannot be explained by a molecular transition in any of the pure constituents. To explain this phenomenon, the dynamic mechanical response of the ternary blends was also simulated theoretically with an interlayer model, which allows the calculation of the viscoelastic properties of a polymer blend with an interphase without the use of any fitting parameters (the basis of the model and the performance of the calculations have been described in detail previously[9,12,13]). It was assumed in the calculations that P(S-*g*-EO) forms a spherical shell, i.e. an interphase, covering spherical PPO particles in a PMMA matrix. The input data in the model are the dynamic shear storage and dynamic shear loss moduli values at different temperatures and frequencies for the constituents, as well as their Poisson ratios. The model predicts an additional, concentration dependent transition in the same temperature range as for the experimental observations. This additional transition was shown to originate from the change in the relative moduli of the constituents in the

* To whom correspondence should be addressed

matrix–interphase–particle structure of the blends and was designated a 'micromechanical transition'.

The position and frequency dependence of the micromechanical transition was shown both experimentally and theoretically to depend on the volume fraction of interphase in the ternary blends, and the micromechanical transition temperature (T_{mm}) was predicted to be strongly dependent on the Poisson ratio of the interphase[10]. The theory also shows that T_{mm} decreases, while the activation energy of the micromechanical transition (E_a) increases, when the copolymer content is increased, in agreement with experiments. The experimental dependence of T_{mm} and E_a was smaller than that predicted by theory, which can, however, be explained by the influence of PPO and PMMA on the properties of the interphase, i.e. that P(S-*g*-EO) is mixed to some extent with the homopolymers in the interphase. The qualitative agreement between experiments and theory on the micromechanical transition is an indirect proof of the existence of an interphase with its own characteristic properties.

The aim of the present work was to compare qualitatively the influence of two P(S-*g*-EO) graft copolymers with different architectures (graft lengths and graft densities) on the properties of PPO/PMMA blends. The morphology, dynamic mechanical and dielectric responses of the blends were determined by different experimental techniques to gain direct and indirect information on the interphase properties of the blends.

EXPERIMENTAL

Materials

The homopolymers used in this study were both commercial products (Scientific Polymer Products) and were used as received. PPO has an approximate $\bar{M}_w$ of 50 kg mol^{-1} and a density of 1060 kg m^{-3}, while PMMA has an approximate $\bar{M}_w$ of 75 kg mol^{-1} and a density of 1200 kg m^{-3}, according to the manufacture. The backbones of the two graft copolymers were first synthesized by a free radical mechanism with styrene and acrylamide, after which the amide groups were used as initiator sites for the polymerization of ethylene oxide. Details of the preparation and characterization of the graft copolymers have been described previously[8,14]. The two graft copolymers are schematically drawn in *Figure 1* and the characteristics of the graft copolymers are presented in *Table 1* [the graft copolymer designated 'P(S-*g*-EO)-5' is equivalent to the 'P(S-*g*-EO)' copolymer used previously[8–11]]. The only difference between the two graft copolymers is the graft length and the distance between the grafts, while the length of the backbones and the weight composition of the copolymers are the same.

Blending procedure

Before blending, the homopolymers were dried overnight at 60°C, while the graft copolymers were dried in a vacuum oven at 40°C for 20 h. Binary and ternary blends were prepared in a Brabender AEV 330 with a chamber volume of 50 cm^3. Blending was performed for 10 min at 260°C (set temperature) with 40 rev min^{-1}. The blends were then cooled at room temperature. PPO/PMMA/copolymer blends with the common composition of 30 volume parts of PPO and 70 volume parts of PMMA were prepared with an additional amount of 0, 1, 2, 5 and 10 volume parts of P(S-*g*-EO)-1 (Φ_1) or P(S-*g*-EO)-5 (Φ_5). Binary PPO/copolymer and PMMA/copolymer blends were prepared with 100 volume parts of homopolymer and 10 volume parts of copolymer by the same procedure. The volume compositions are based on the densities at room temperature (ρ_{PPO} = 1060 kg m^{-3}, ρ_{PMMA} = 1200 kg m^{-3} and ρ_{copol} = 1110 kg m^{-3}).

P(S-g-EO)-1

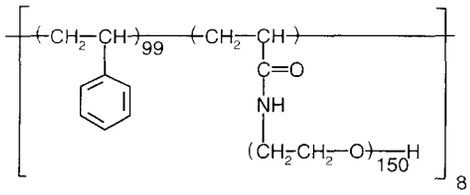

P(S-g-EO)-5

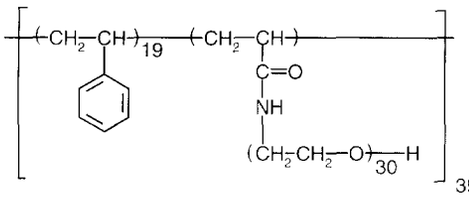

Figure 1 A schematic drawing of the graft copolymers P(S-*g*-EO)-1 and P(S-*g*-EO)-5. The numbers 99, 150 and 8, as well as 19, 30 and 39, are average values

Table 1 The characteristics of the PS/PEO graft copolymers

Characteristic	P(S-*g*-EO)-1	P(S-*g*-EO)-5[a]
Acrylamide in the backbone (mol%)	1	5
PEO content (wt%)	38	39
T_m of PEO (°C)	56	57
T_c of PEO (°C)	35	35
M_n (backbone) (kg mol^{-1})	80	80
M_n (side chains) (kg mol^{-1})	6.5	1.3

[a] Equivalent to the graft copolymer previously[8–11] designated as 'P(S-*g*-EO)'

Instrumentation

SEM experiments were performed with a Zeiss DSM 940A to study the phase structure of the blends. Brabender samples were first fractured in liquid nitrogen, then sputter-coated with a thin layer of gold and finally analysed under the microscope with an acceleration voltage of 5–10 kV. The blends were also studied with a Philips CM200 transmission electron microscope (TEM). Slices with an approximate thickness of 100 nm were first cut at −120°C and then stained with RuO_4 for 15 min in order to obtain a contrast in the micrographs. The samples were examined with an acceleration voltage of 120 kV.

Dynamic mechanical spectroscopy (DMS) measurements were performed with a Rheometrics RDA II instrument in the oscillatory mode. Measurement were performed at temperatures ranging from −80 to 250°C and with angular frequencies, ω, from 0.001 to 500 rad s^{-1}. Solid state samples, with the shape of a rectangular parallelepiped and the approximate dimensions of 30× 12 × 2 mm^3, were subjected to a maximum shear strain of 0.1%, except the PMMA/P(S-*g*-EO)-5 100/10 blend (maximum shear strain 0.2%). The melt state samples, with the shape of a cylinder with a diameter of 25 mm

and an approximate thickness of 2 mm, were subjected to a maximum shear strain of 10%. All measurements were performed by starting at a lower temperature and then increasing the temperature, except the measurements in the temperature range from 25 to 150°C, which were also performed by starting at 150°C and then decreasing the temperature. This procedure was followed in order to eliminate the effect of any crystalline EO above the onset of crystallization T_c. T_c was determined to be approximately 35°C for both P(S-*g*-EO)-1 and P(S-*g*-EO)-5 by cooling the pure copolymers from 130°C at a rate of 5°C min^{-1} in a Perkin-Elmer System 7 differential scanning calorimeter.

Dielectric analysis was performed in the frequency range 125 mHz–4 MHz with a Schlumberger type 1260 frequency response analyser, interfaced with a parallel plate sample capacitor via a custom-made electrometer, and a Hewlett Packard type 4275A LCR analyser. The measurements were performed on samples with dimensions $40 \times 40 \times 2\,mm^3$, as a function of temperature between 22 and 150°C, at 1°C intervals. Two gold electrodes with a diameter of 3.5 cm were sputtered on the dielectric samples.

Modulated differential scanning calorimetry (m.d.s.c.) experiments[15] were performed with a TA Instruments 2920 apparatus at temperatures from −100 to +250°C. The heating and cooling rate was 4°C min^{-1} and a modulation amplitude of 0.5°C and a period of 60 s were used. Helium was used as purge gas (at 25 ml min^{-1}).

RESULTS AND DISCUSSION

The pure constituents and the binary homopolymer/copolymer blends

The dynamic shear storage modulus, $G'(\omega, T)$, and the dynamic shear loss modulus, $G''(\omega, T)$, are given for PPO, PMMA, P(S-*g*-EO)-1 and P(S-*g*-EO)-5 at different temperatures ($\omega = 0.02321$ rad s^{-1}) in *Figure 2* (measurements were performed both in the solid and the melt state). It can be observed that PMMA and PPO have approximately constant moduli values up to their glass transition temperatures (T_g). The two graft copolymers behave quite differently (the data for the copolymers in *Figure 2* represent the properties in the amorphous state, as experiments were performed from higher to lower temperatures above the onset of crystallization using frequency–temperature superposition). P(S-*g*-EO)-5 has a G'' maximum at −56°C ($\omega = 1$ rad s^{-1}) when measurements are performed from lower to higher temperatures. This is likely to correspond to glass transition of the amorphous PEO side chains. When measurements are performed in the melt state (i.e. from 135 to 40°C, where the lower end data were extended to 25°C by measuring at lower angular frequencies with the use of time–temperature superposition), the modulus is much lower than the moduli of the homopolymers, and no G'' maximum can be observed in this temperature range. P(S-*g*-EO)-1, on the other hand, is much stiffer than P(S-*g*-EO)-5 and has a detectable G'' maximum at 76°C ($\omega = 1$ rad s^{-1}), which probably corresponds to the glass transition of the PS segments. However, a transition at lower temperatures corresponding to the glass transition of PEO cannot be detected, which indicates that the amorphous part of PEO (in the solid state) is small in P(S-*g*-EO)-1. The difference between the two graft

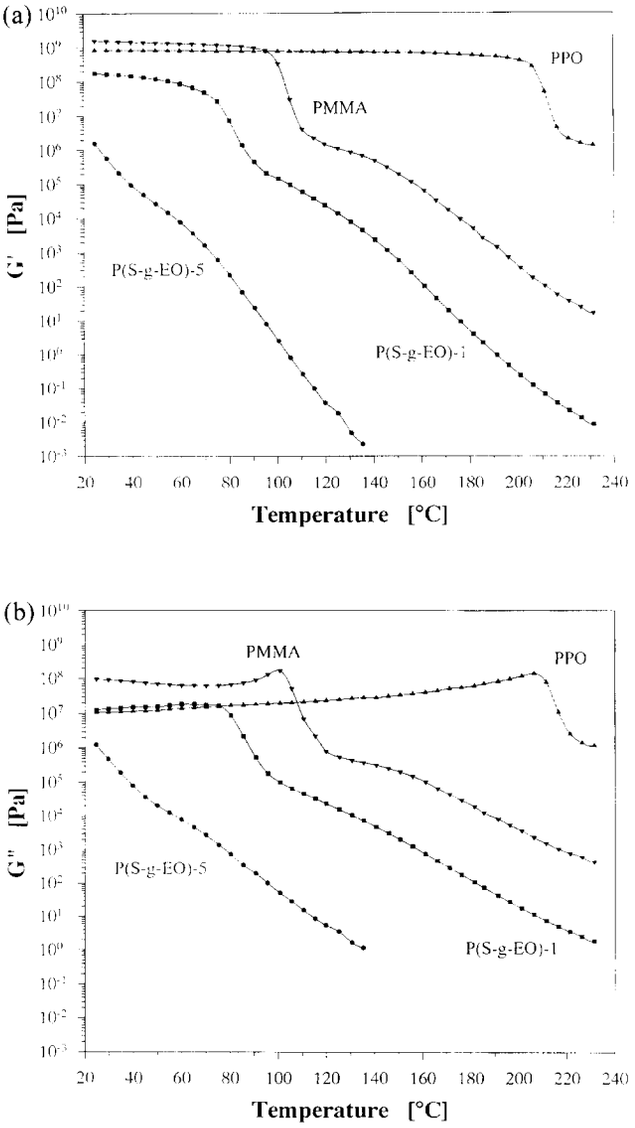

Figure 2 Experimental (a) $G'(\omega, T)$ and (b) $G''(\omega, T)$ values of (▲) PPO, (▼) PMMA, (■) P(S-*g*-EO)-1 and (●) P(S-*g*-EO)-5 in the temperature range 25–230°C ($\omega = 0.02321$ rad s^{-1})

copolymers can be explained by their different architectures. The lower modulus in P(S-*g*-EO)-5 can be explained by the short distance between the flexible PEO grafts (an average of one graft per 40 carbon atoms in the backbone), which increases the mobility of the backbone. The great flexibility of the backbone chains in P(S-*g*-EO)-5 can also explain why no glass transition can be detected for the PS segments. P(S-*g*-EO)-1 has longer side chains and fewer branch points (an average of one graft per 200 C atoms in the backbone) and behaves, therefore, more like a normal block or graft copolymer.

In *Figure 3*, the dynamic shear loss modulus, G'', is plotted as a function of temperature ($\omega = 0.02321$ rad s^{-1}) for pure PMMA and PPO homopolymers, as well as for the binary PMMA/P(S-*g*-EO)-1 (100/10), PMMA/P(S-*g*-EO)-5 (100/10), PPO/P(S-*g*-EO)-1 (100/10) and PPO/P(S-*g*-EO)-5 (100/10) blends. The figure shows that only one major transition can be observed in each binary blend and that the transitions are shifted to lower temperatures, as compared with the pure homopolymers. This indicates that the PS and PEO parts of both the graft copolymers interact with PPO and PMMA, respectively,

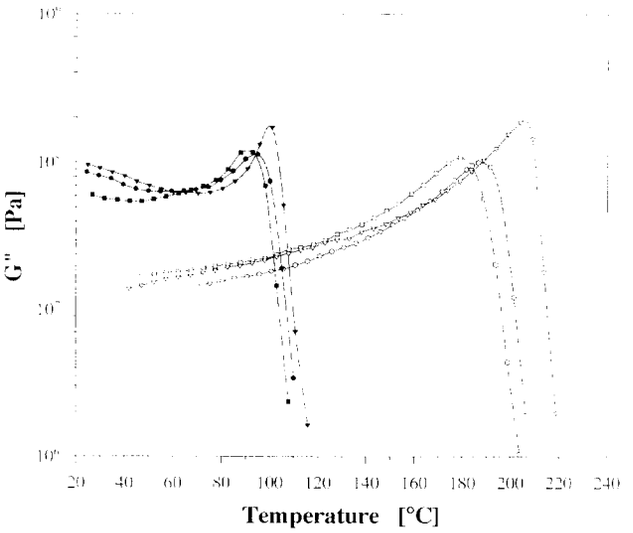

Figure 3 Experimental $G''(\omega, T)$ values for (▲) PMMA and (▽) PPO, as well as for the binary (■) PMMA/P(S-*g*-EO)-1 100/10, (●) PMMA/P(S-*g*-EO)-5 100/10, (□) PPO/P(S-*g*-EO)-1 100/10 and (○) PPO/P(S-*g*-EO)-5 100/10 blends ($\omega = 0.02321$ rad s^{-1})

i.e. that the graft copolymers are at least partially miscible with both the homopolymers, as previously concluded[8–10] for P(S-*g*-EO)-5. This is also in agreement with SEM images of the binary blends, which do not indicate any phase separation. However, it cannot be excluded from these experiments that the copolymers form micelles in the homopolymers. *Figure 3* also shows that P(S-*g*-EO)-1 reduces the T_g of both PMMA and PPO more than does P(S-*g*-EO)-5. As the two graft copolymers have approximately the same composition on a weight basis, this indicates that the structure of P(S-*g*-EO)-1, with longer and more separated PS and PEO segments, is favourable for interacting with PPO and PMMA.

Ternary PPO/PMMA/P(S-g-EO) blends

SEM images of fracture surfaces of the PPO/PMMA (30/70), PPO/PMMA/P(S-*g*-EO)-1 (30/70/5) and PPO/PMMA/P(S-*g*-EO)-5 (30/70/5) blends are presented in *Figure 4*. In the PPO/PMMA (30/70) blend, the PPO phase can be observed as inclusions in the PMMA matrix. This structure, with dispersed PPO particles, is also preserved when the copolymers are added, but it can be clearly observed that both the copolymers reduce the size of the dispersed PPO phase. The number average dimensions of the particles were estimated from SEM images of the fracture surfaces of the PPO/PMMA/P(S-*g*-EO)-1 30/70/Φ_1 and PPO/PMMA/P(S-*g*-EO)-5 30/70/Φ_5 blends ($\Phi_1 = \Phi_5 = 0$, 1, 2, 5 and 10). The results are presented in *Figure 5* (approximately 30 particles or holes were measured for each sample), where the error bars represent the standard deviation, and show that the average dimensions decrease continuously with an increasing amount of added copolymer. It can also be observed that the average dimensions of the PPO/PMMA/P(S-*g*-EO)-1 30/70/Φ_1 blends are smaller than for the PPO/PMMA/P(S-*g*-EO)-5 30/70/Φ_5 blends with the same Φ value. This means that P(S-*g*-EO)-1 is more efficient in reducing the phase dimension, i.e. is a more efficient compatibilizer than P(S-*g*-EO)-5. In a comparison with the results of the binary homopolymer/copolymer blends, it can be concluded that the copolymer that is most able to be mixed with the homopolymers is a more efficient compatibilizer. The results of this work are in agreement with experimental and theoretical studies, which have shown that the reduction of the dispersed phase size increases as the molecular masses of the copolymer segments increase in relation to the molecular masses of the homopolymers[16–21].

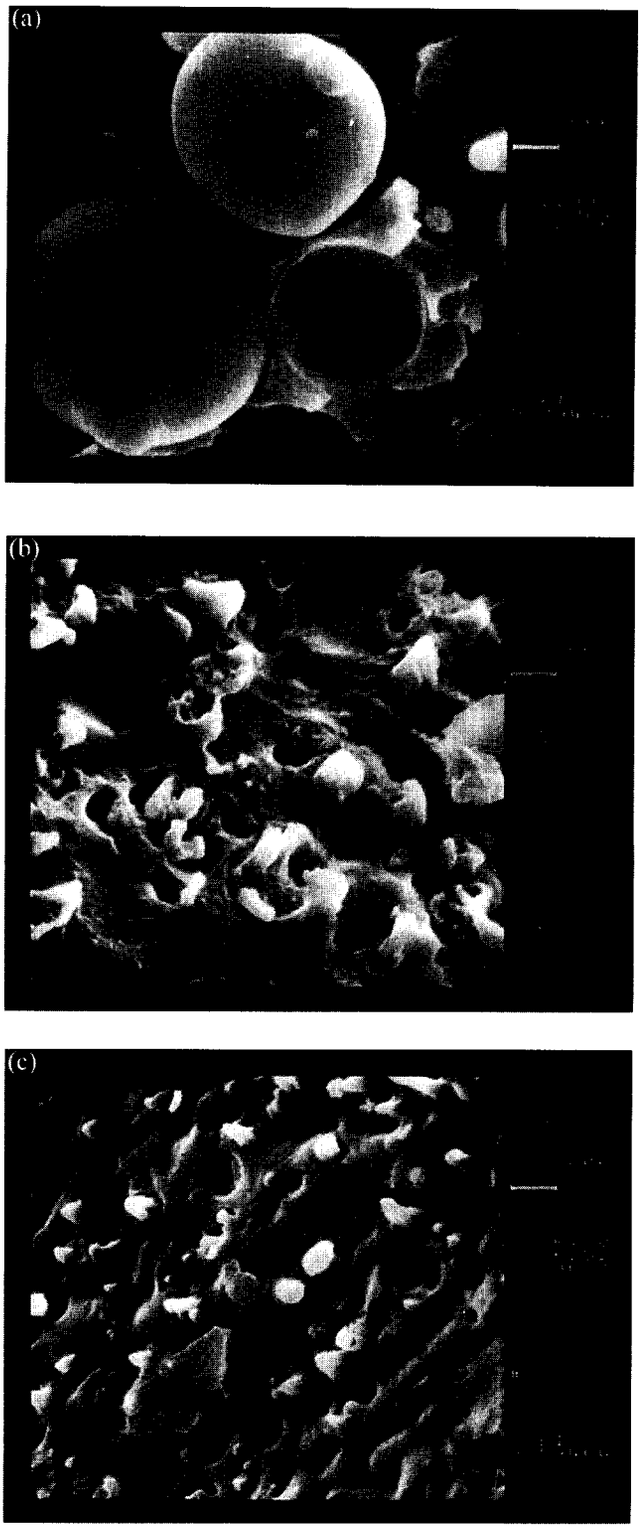

Figure 4 SEM micrographs of fracture surfaces of (a) PPO/PMMA 30/70, (b) PPO/PMMA/P(S-*g*-EO)-1 30/70/5 and (c) PPO/PMMA/P(S-*g*-EO)-5 30/70/5 blends

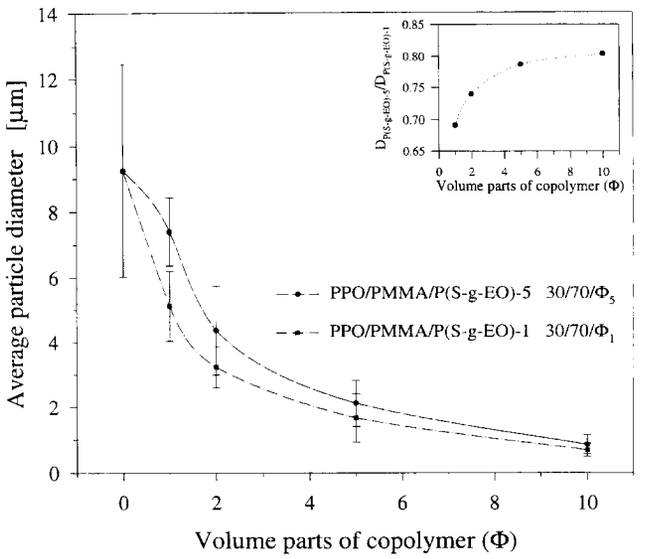

Figure 5 Average particle diameter in the PPO/PMMA/P(S-*g*-EO) blends, as determined from SEM micrographs of fracture surfaces. The error bars represent the standard deviations. In the upper right corner, the quotients between the average particle diameters of the PPO/PMMA/P(S-*g*-EO)-1 30/70/Φ_1 and PPO/PMMA/P(S-*g*-EO)-5 30/70/Φ_5 blends are given

In the upper right corner of *Figure 5*, the quotient between the average phase dimension of the PPO/PMMA/P(S-*g*-EO)-1 (30/70/Φ_1) and the PPO/PMMA/P(S-*g*-EO)-5 (30/70/Φ_5) blends is given for each Φ value. The quotient is less than 1 because P(S-*g*-EO)-1 reduces the dispersed phase dimension more than P(S-*g*-EO)-5 does in the PPO/PMMA/copolymer (30/70/Φ) blends. It can be observed that the quotient continuously increases from 0.69 to 0.80 when Φ is increased from 1 to 10. The results thus show that the relative size reduction of P(S-*g*-EO)-1 is larger when Φ is small. This indicates that the structure of a compatibilizer is more important when it is added in small amounts, which has also been shown to be the case in PS/PMMA/P(S-*b*-MMA) blends with different molecular masses of the P(S-*b*-MMA) block copolymer[22].

TEM experiments were performed to study the interphase in the ternary blends. *Figure 6a* shows a TEM image of the PPO/PMMA/P(S-*g*-EO)-5 (30/70/2) blend. The image shows a matrix of PMMA (light grey) and dispersed PPO particles (dark grey). The PPO parts, which have irregular shapes, have a size of 2–16 μm and contain some PMMA inclusions. It can be observed that the PPO particles are surrounded by an interlayer (middle grey) with a thickness of 0–600 nm. This is direct proof of the existence of a separate phase between the PMMA and PPO phase. We have previously[8] estimated the thickness of the interphase in all the PPO/PMMA/P(S-*g*-EO)-5 30/70/Φ_5 blends to be 47 ± 10 nm, by assuming that all, and only, the added P(S-*g*-EO)-5 forms an interphase around spherical PPO particles with the diameter given by the averages in *Figure 5*. This is smaller than what is observed experimentally by TEM for most of the particles in *Figure 6a*. An explanation for this may be that the interlayer, which seems to form a separate phase between PPO and PMMA, contains not only P(S-*g*-EO)-5, but also some amount of PMMA and/or PPO. This assumption is supported by n.m.r. and DMS observations in previous studies[8]. A contributory explanation of the observed interphase thickness can be

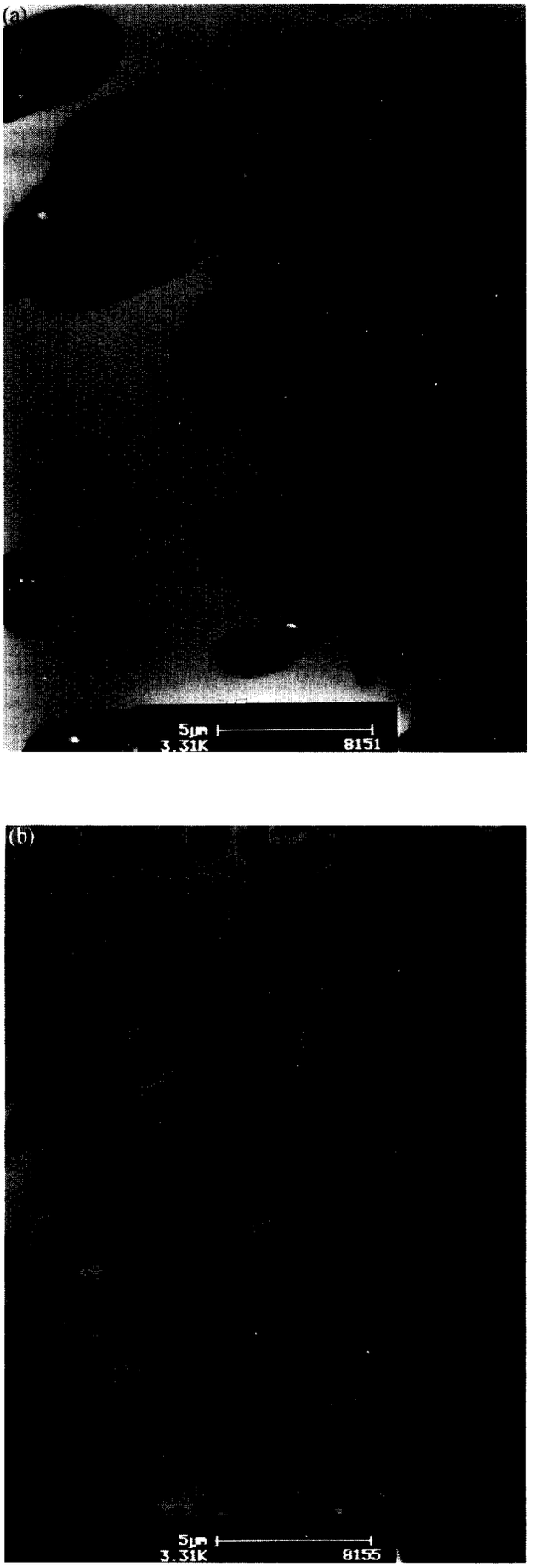

Figure 6 TEM micrographs of the PPO/PMMA/P(S-*g*-EO)-5 (a) 30/70/2 and (b) 30/70/10 blends

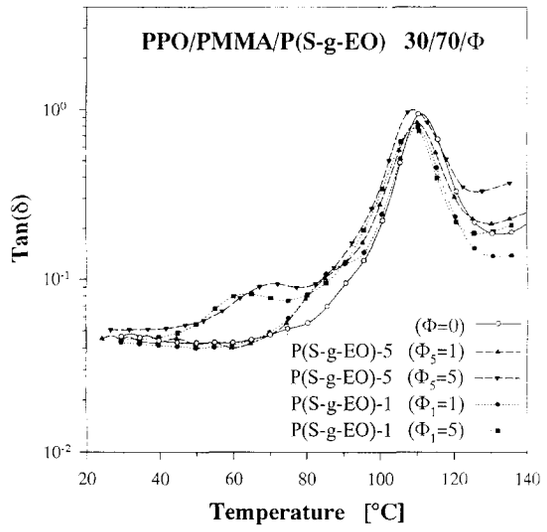

Figure 7 Experimental tan δ *versus* temperature values for the PPO/PMMA 30/70, PPO/PMMA/P(S-*g*-EO)-1 30/70/1, PPO/PMMA/P(S-*g*-EO)-1 30/70/5, PPO/PMMA/P(S-*g*-EO)-5 30/70/1 and PPO/PMMA/P(S-*g*-EO)-5 30/70/5 blends (T = 25–135°C and ω = 0.02121 rad s^{-1})

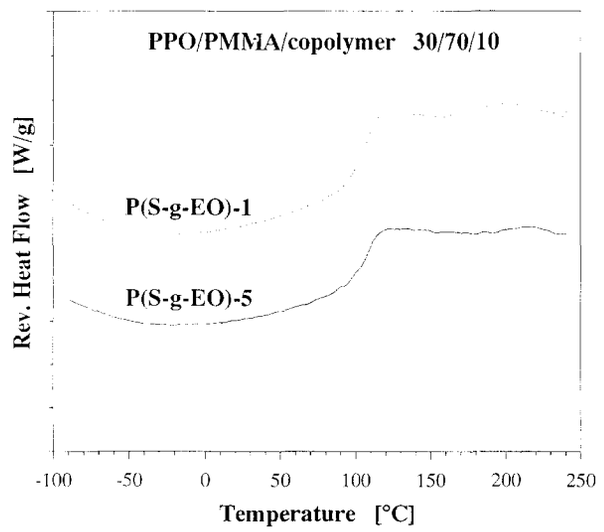

Figure 8 The reversing heat flow for the PPO/PMMA/P(S-*g*-EO)-1 30/70/10 and PPO/PMMA/P(S-*g*-EO)-1 30/70/10 blends, as measured by m.d.s.c.

that, when the particles show a size distribution rather than a common size (the volume fractions are constant), the total interface area is smaller. This means that the interphase around particles of varying sizes should be thicker than the interphase around particles of equal size when the volume fraction and number average particle diameter are equal. In the PPO/PMMA/P(S-*g*-EO)-5 30/70/10 blend, the PPO particles are finer and more regularly dispersed in the PMMA matrix, which is shown in *Figure 6b*. The dark PPO parts in the TEM image have a size of approximately 0.5–2.0 μm. The PPO particles in this blend are also surrounded by an interlayer (middle grey), which to a large extent consists of P(S-*g*-EO)-5. It also seems as though another separate phase, observed as particles with the same middle grey colour as the interphase, is formed in the PMMA matrix in this blend. This is likely to be a copolymer-rich phase, which is created when the added copolymer content is large. Because the contrast is not as good for this blend, it is difficult to estimate the dimensions of this phase. Besides the larger phases described above, there are smaller particles in the PMMA matrix with dimensions of 50–100 nm, but it cannot be determined whether these consist of P(S-*g*-EO)-5 and/or PPO.

TEM experiments were also performed with the PPO/PMMA/P(S-*g*-EO)-1 30/70/2 and 30/70/10 blends. The images show a morphology similar to the PPO/PMMA/P(S-*g*-EO)-5 system with PPO particles surrounded by an interphase in a PMMA matrix. The thickness of the interphase is, however, difficult to estimate because the contrast is not good in these images. A difference between the two systems is that the phase size in the blend with two volume parts of added P(S-*g*-EO)-1 is clearly smaller (1–6 μm) than the corresponding blend with P(S-*g*-EO)-5. The fine phase with the size 50–100 nm cannot be observed in any of the blends compatibilized by P(S-*g*-EO)-1, which may be an indication that P(S-*g*-EO)-1 is more concentrated at the interphase than P(S-*g*-EO)-5 in the PPO/PMMA system.

Dynamic mechanical results (tan δ *versus* temperature) of the PPO/PMMA 30/70 blend and the ternary blends with 1 and 5 volume parts of copolymer added are shown in *Figure 7*. The heterogeneous PPO/PMMA 30/70 blend shows an expected behaviour, with two tan δ maxima corresponding to the glass transitions of PMMA (104°C) and PPO (213°C, not shown in the figure). However, when any of the copolymers are added, an additional transition at temperatures between 60 and 100°C can be detected. The additional transition temperature decreases when the copolymer content is increased. It should be noted that the additional transition in both systems appears where no single constituent has a molecular transition [P(S-*g*-EO)-1 shows a tan δ maximum at +87°C (ω = 0.02321 rad s^{-1}), which is clearly above the maxima for the blends with five volume parts of added P(S-*g*-EO)-1]. We have previously described the dynamic mechanical behaviour of the ternary PPO/PMMA/P(S-*g*-EO)-5 30/70/Φ_5 blends[8–10]. By comparing experiments with theoretical calculations using an interlayer model[12–13], which assumes that P(S-*g*-EO)-5 forms an interphase around spherical PPO particles in the PMMA matrix (in

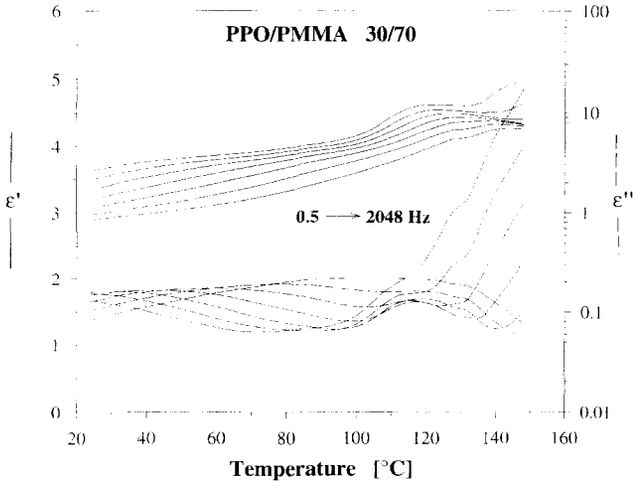

Figure 9 Experimental ϵ' (solid lines) and ϵ'' (dashed lines) values for the PPO/PMMA 30/70 blend. The lines represent data at 0.5, 2, 8, 32, 128, 512 and 2048 Hz

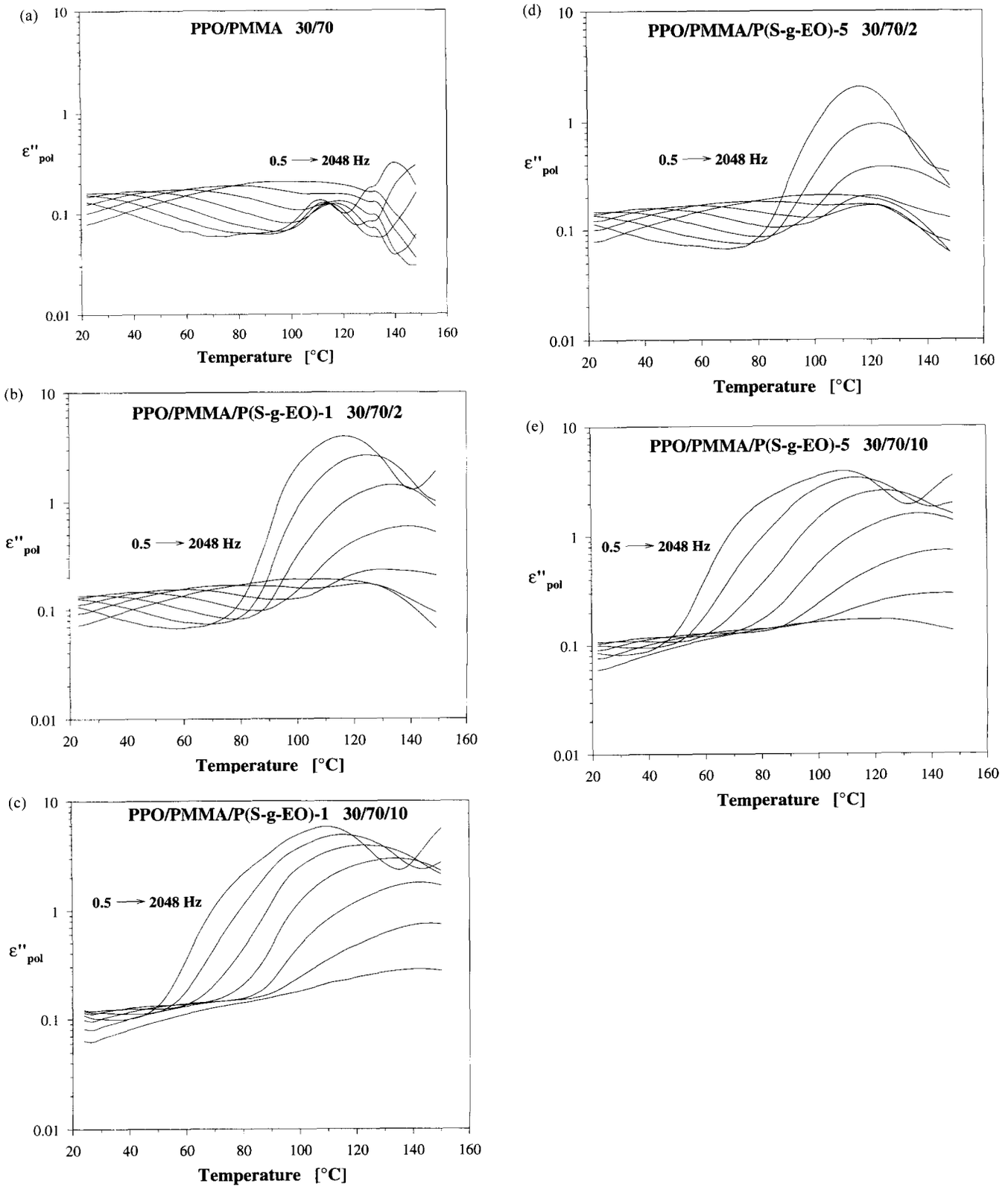

Figure 10 Calculated ϵ''_{pol} values for the (a) PPO/PPMA 30/70, (b) PPO/PMMA/P(S-*g*-EO)-1 30/70/2, (c) PPO/PMMA/P(S-*g*-EO)-1 30/70/10, (d) PPO/PMMA/P(S-*g*-EO)-5 30/70/2 and (e) PPO/PMMA/P(S-*g*-EO)-5 30/70/10 blends. The lines represent data at 0.5, 2, 8, 32, 128, 512 and 2048 Hz

agreement with the TEM results in this work), it was concluded that an additional 'micromechanical transition' can be observed at temperatures below the glass transition of PMMA when P(S-*g*-EO)-5 is added. This was shown to originate from the change in relative moduli of the constituents, due to the sharp decrease of the modulus of the interphase, in the matrix–interphase–particle structure of the blends.

To verify further the origin of the additional transition in the ternary blends, m.d.s.c. experiments were performed. *Figure 8* shows the reversing heat flow during cooling for the two systems with 10 volume parts of copolymer added to a PPO/PMMA 30/70 blend. The figure shows that only one clear molecular transition can be detected between −80 and +150°C in each blend, corresponding to the T_g of PMMA. A weak transition at

180–220°C can also be observed, which may represent the T_g of PPO. However, no transition corresponding to the tan δ maxima at approximately +60°C in these two blends can be detected by m.d.s.c. experiments. Hence, these measurements show no indication of a molecular transition in the region of the additional transition observed with DMS, which supports the conclusion of a micromechanical transition in the ternary blends.

As a complement to the investigation of the dynamic mechanical properties of the blends, a study was made of the influence of the copolymers on the dielectric properties. The dielectric constant, $\epsilon'(\omega, T)$, and the dielectric loss index, $\epsilon''(\omega, T)$, of a PPO/PMMA 30/70 blend are depicted in *Figure 9* as a function of both temperature and frequency. Two distinct retardation processes can be observed from the $\epsilon''(\omega, T)$ values in the measured temperature region. At low temperatures, the β-transition of the PMMA phase is detected from the dielectric loss index. Between 100 and 130°C, the main α-transition related to the glass–rubber transition of the PMMA phase is clearly visible. At temperatures above the glass–rubber transition of the PMMA matrix, the matrix conductivity increases sharply, which gives a strong increase in dielectric losses, especially at the lowest frequencies.

As the dielectric losses are contributed to by both polarization and conductivity losses, we have determined the polarization contribution from the dielectric constant, as measured at a geometric series of frequencies centred around the frequency of interest, by using a numerical algorithm for the Kramers–Kronig tranform[23]. The dielectric polarization losses, $\epsilon''_{pol}(\omega, T)$, of a PPO/PMMA 30/70 blend are depicted in *Figure 10a*. After applying the Kramers–Kronig transform, the α-transition of PMMA is clearly visible as a maximum in ϵ''_{pol} at 100–130°C. The retardations observed above the glass–rubber transition of PMMA can be attributed to macroscopic charge effects due to interfacial blocking of charge transport between the PMMA and the PPO phases.

The compatibilizers drastically alter the experimental dielectric response of the blends. In *Figures 10b–e*, the dielectric polarization losses are depicted as a function of temperature for the PPO/PMMA 30/70 blends with 2 and 10 volume parts of P(S-*g*-EO)-1 and P(S-*g*-EO)-5 compatibilizers added. With decreasing frequency, two strong polarization processes become visible in the compatibilized blends at decreasing temperatures. Considering the strength of the observed transitions, a polarization process due to permanent dipoles seems unlikely. Instead, this behaviour is at least partly characteristic of macroscopic or Maxwell–Wagner–Sillars (MWS) interfacial polarization processes, which are caused by the build-up of space charges at interfaces in the material[24]. A necessary condition for such a charge build-up is the coexistence of a conductive phase in the material with a less conductive phase. Obviously, a transition from the glassy to liquid phase of at least one of the constituents satisfies the condition through a sharp increase of ion conductivity. Hence, the polarization process at higher temperatures (overlapping the PMMA transition above 100°C), where the interphase material is conductive and the PMMA phase passes its glass–rubber transition, may be attributed to a MWS interfacial polarization process caused by the charge build-up between the PMMA phase and the copolymer-rich interphase.

Analogues to the effect of a conductive water layer at the interface of glass spheres-filled polyethylene composites[25–27], which give rise to a strong microdielectric transition, with temperature and frequency positions strongly dependent on the amount of water and its conductivity, we also expect at least one clear transition for the compatibilized blends. The lowest observed transition (at 60–100°C) in each ternary blend is attributed to the microdielectric transition caused by the change of conductivity (and thus dielectric losses) in the interphase (with its specific volume fraction) with increasing temperature. Analogous to the mechanical experiments, this transition shifts to lower temperatures with increasing volume fraction of compatibilizer, thus becoming more separated from the MWS effect due to the PMMA phase. The phenomena with microdielectric and micromechanical transitions are thus comparable.

CONCLUSIONS

We have in this work studied the effect of two graft copolymers on the dynamic mechanical and dielectric response, morphology and interphase properties in different blends containing PPO and PMMA. The two graft copolymers consist of PS backbones of equal lengths and PEO grafts with different lengths and graft densities, but the same total weight composition.

We have shown that both graft copolymers are at least partially miscible with PPO and PMMA. DMS measurements on binary PPO/copolymer and PMMA/copolymer blends show that the glass transition of each homopolymer is shifted to lower temperatures when P(S-*g*-EO)-1 or P(S-*g*-EO)-5 is blended with PPO or PMMA. The reduction in T_g is larger when P(S-*g*-EO)-1 is mixed with either PPO or PMMA, which indicates that interactions in this case are favoured by longer and more separated grafts.

SEM experiments show that the dispersed PPO phase size in PPO/PMMA 30/70 blends is reduced by the addition of any of the copolymers, but the reduction is more efficient when P(S-*g*-EO)-1 (long but fewer grafts) is added. Whether the graft length or the distance between the grafts is most important for this effect is difficult to say, but it is reasonable to assume that both factors influence the compatibilization. It can be concluded that the compatibilizing efficiency is related to the ability of the copolymers to interact with the homopolymers. TEM experiments show that an interlayer is formed around the PPO phase when P(S-*g*-EO)-1 or P(S-*g*-EO)-5 is added to the PPO/PMMA 30/70 blends. Previous DMS and n.m.r. experiments strongly suggest that the interlayer is a copolymer-rich phase.

DMS experiments show that the ternary blends of both systems have a similar micromechanical transition at temperatures in the range 60–100°C, which originates from the presence of interphases with certain properties. The micromechanical transition temperature decreases when the copolymer content is increased for both systems, which can also be expected from theoretical simulations using an interlayer model with a copolymer forming an interphase around spherical PPO particles in a PMMA matrix.

Dielectric measurements show that the copolymers strongly influence the dielectric response of the PPO/PMMA/P(S-*g*-EO) blends. A MWS interfacial polarization process can be detected above 100°C when any of

the copolymers are added to a PPO/PMMA 30/70 blend. This is caused by charge build-up between the PMMA phase and the copolymer-rich interphase. At lower temperatures (60–100°C), a microdielectric transition is detected in the ternary blends, which is caused by the increase in dielectric losses of the interphase with increasing temperature.

It can be concluded that the effects of P(S-*g*-EO)-1 and P(S-*g*-EO)-5 on the dynamic mechanical and dielectric properties are quite similar. An interpretation of this is that the mixture between the copolymers and the homopolymers in the interphases results in quite similar interphase properties for the two systems, even though the properties of the pure copolymers are dissimilar.

ACKNOWLEDGEMENTS

The authors are very grateful to the National Swedish Board for Industrial and Technical Development (NUTEK) for financial support of this work. We also gratefully acknowledge Patric Jannasch at the Lund Institute of Technology (Sweden) for synthesizing the graft copolymers, and Monique Walet at DSM Research (The Netherlands) for performing the TEM experiments. Finally, we would like to thank Els Verdonck and Bruno van Mele at the Free University of Brussels (Belgium) for performing the m.d.s.c. experiments, and Cor Koning at DSM Research (The Netherlands) for valuable discussions.

REFERENCES

1 Fayt, R., Jerome, R. and Teyssie, P. *J. Polym. Sci.: Polym. Lett. Edn.* 1986, **24**, 25
2 Vilgis, T. A. and Noolandi, J. *Macromolecules* 1990, **23**, 2941
3 Brown, H. R., Char, K., Deline, V. R. and Green, P. F. *Macromolecules* 1993, **26**, 4155
4 Brown, H. R., Char, K. and Deline, V. R. *Macromolecules* 1993, **26**, 4164
5 Chen, C. C. and White, J. L. *Polym. Eng. Sci.* 1993, **33**, 923
6 Gleinser, W., Friedrich, C. and Cantow, H.-J. *Polymer* 1994, **35**, 128
7 Tang, T. and Huang, B. *Polymer* 1994, **35**, 281
8 Eklind, H., Schantz, S., Maurer, F. H. J., Jannasch, P. and Wesslén, B. *Macromolecules* 1996, **29**, 984
9 Eklind, H. and Maurer, F. H. J. *Polymer* 1996, **37**, 2641
10 Eklind, H. and Maurer, F. H. J. *J. Polym. Sci.: Polym. Phys. Edn.* 1996, **34**, 1569
11 Kvist, L., Bengtsson, P. and Bertilsson, H. *Polym. Networks Blends* (in press)
12 Maurer, F. H. J. in 'Polymer Composites' (Ed. B. Sedlacek), W. de Gruyter, Berlin, 1986, p. 399
13 Maurer, F. H. J. in 'Controlled Interphases in Composite Materials' (Ed. H. Ishida), Elsevier, New York, 1990, pp. 491–504
14 Jannasch, P. and Wesslén, B. *J. Polym. Sci., Part A: Polym. Chem.* 1993, **31**, 1519
15 Reading, M. *Trends Polym. Sci.* 1993, **1**, 248
16 Inoue, T., Soen, T., Hashimoto, T. and Kawai, H. *Macromolecules* 1970, **3**, 87
17 Noolandi, J. and Hong, K. M. *Macromolecules* 1982, **15**, 482
18 Noolandi, J. and Hong, K. M. *Macromolecules* 1984, **17**, 1531
19 Vilgis, T. A. and Noolandi, J. *Macromolecules* 1990, **23**, 2941
20 Riess, G., Kohler, J., Tournut, C. and Banderet, A. *Makromol. Chem.* 1967, **101**, 58
21 Riess, G. and Jolivet, Y. in 'Copolymers, Polyblends and Composites' (Ed. N. A. J. Platzer), American Chemical Society, New York, 1975, pp. 243–256
22 Thomas, S. and Prud'homme, R. E. *Polymer* 1992, **33**, 4260
23 Steeman, P. A. M. Ph. D. Thesis, Delft University, The Netherlands, 1992
24 Sillars, R. W. *J. Inst. Electr. Eng.* 1937, **80**, 378
25 Steeman, P. A. M. and Maurer, F. H. J. *Colloid Polym. Sci.* 1990, **268**, 315
26 Steeman, P. A. M., Maurer, F. H. J. and van Es, M. Polymer 1991, **31**, 523
27 Steeman, P. A. M., Baetsen, J. H. F. and Maurer, F. H. J. *Polym. Eng. Sci.* 1992, **32**, 351